Thin Film PZT-Based PMUT Arrays for Deterministic Particle Manipulation

Christopher Cheng, *IEEE, Member,* Ajay Dangi, *Member, IEEE,* Liqiang Ren, Sudhanshu Tiwari, Robert Benoit, *IEEE, Member,* Yongqiang Qiu, *IEEE, Member,* Holly S. Lay, *Member, IEEE,* Sumit Agrawal, Rudra Pratap, *Senior Member, IEEE,* Sri-Rajaesekhar Kothapalli, Thomas Mallouk, Sandy Cochran, *Member, IEEE,* Susan Trolier-McKinstry, *Fellow, IEEE*

***Abstract*—Lead zirconate titanate (PZT) based piezoelectric micromachined ultrasonic transducers (PMUTs) for particle manipulation applications were designed, fabricated, characterized and tested. The PMUTs had a diaphragm diameter of 60 µm, a resonant frequency of ~ 8 MHz and an operational bandwidth of 62.5%. Acoustic pressure output in water was 9.5 kPa at 7.5 mm distance from a PMUT element excited with a unipolar waveform at 5 V_{pp}. The element consisted of 20 diaphragms connected electrically in parallel. Particle trapping of 4 µm silica beads was shown to be possible with 5 V_{pp} unipolar excitation. Trapping of multiple beads by a single element and deterministic control of particles via acoustophoresis without the assistance of microfluidic flow were demonstrated. It was found that the particles move towards diaphragm areas of highest pressure, in agreement with literature and simulations. Unique bead patterns were generated at different driving frequencies and were formed at frequencies up to 60 MHz, much higher than the operational bandwidth. Levitation planes were generated above 30 MHz driving frequency.**

***Index Terms*—Acoustic tweezing, arrays, MEMS, particle manipulation, PMUT, ultrasound transducers**

I. Introduction

There is growing interest in devices to independently and deterministically manipulate microscale objects, particularly in the biological sciences. Various contact and non-contact technologies have been developed to meet this demand. Non-contact methods are strongly preferred in biology as they maintain the integrity of cells and minimize interference with intercellular and intracellular processes [1, 2].

Of the reported non-contact methods, optical tweezers, dielectrophoresis, magnetophoresis, and acoustophoresis have been used for particle manipulation. Acoustophoresis is particularly attractive for biological applications as it does not require labelling, has no known toxic effects, and can maintain cell integrity during operation [3, 4, 5, 6, 7].

Many ultrasonic transducer designs have been explored for acoustic tweezing, as shown in Fig. 1. Unlike transducers for imaging, these are required only to transmit energy not to act additionally as receivers. Conventional transducers based on bulk piezoelectric materials or piezocomposites with front and back electrodes, Fig. 1(a), often have a matching layer to enhance energy transfer between the high acoustic impedance of the device and the low acoustic impedance of the medium. A backing layer may also be used to dampen ringing or reflect acoustic energy back to the front surface. However, conventional transducer structures constrain the geometry and hence operating frequencies and electrical impedance matching of the small elements in two dimensional arrays for particle manipulation applications.

In contrast, micromachined ultrasonic transducers (MUTs) prepared using microelectromechanical systems (MEMS) fabrication techniques allow ultrasonic arrays to be configured flexibly, with high spatial resolution, from many small diaphragms. They also offer intrinsically good acoustic matching and operating bandwidth and the potential for excellent electrical impedance matching. Two distinct platform technologies have emerged: capacitive micromachined ultrasonic transducers (CMUTs) and piezoelectric micromachined ultrasonic transducers (PMUTs).

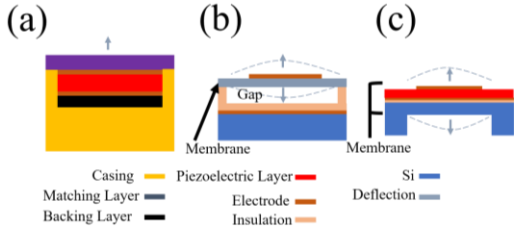

Fig. 1. Typical architectures of (a) a bulk piezoelectric transducer, (b) a capacitive micromachined ultrasonic transducer and (c) a piezoelectric micromachined ultrasonic transducer (after [8]).

Manuscript sent March 7, 2019. This work was supported in part by The Center for Nanoscale Science, a Materials Research Science and Engineering Center (MRSEC) supported by the National Science Foundation under grant DMR-1420620. Christopher Cheng was supported by the National Defense Science & Engineering Graduate (NDSEG) Fellowship Program. Ajay Dangi postdoctoral fellowship was supported by the National Institute of Biomedical Imaging and Bioengineering (NIBIB) center of National Institute of Health under Grant R00EB017729-04 awarded to Dr. Kothapalli.

C. Y. Cheng and S. E. Trolier-McKinstry are with the Department of Materials Science and Engineering and the Materials Research Institute, Pennsylvania State University, PA 16802, USA (e-mail: cyc5@psu.edu; set1@psu.edu).

A. Dangi, S. Agrawal, and S. Kothapalli are with the Department of Biomedical Engineering, Pennsylvania State University, PA 16802, USA (e-mail: axd571@psu.edu; sua347@psu.edu; szk416@psu.edu).

L. Ren is with the Department of Engineering Science and Mechanics, Pennsylvania State University, PA 16802, USA (e-mail: lzr144@psu.edu).

T. Mallouk is with the Department of Chemistry, Pennsylvania State University, PA 16802, USA (e-mail: lzr144@psu.edu; tem5@psu.edu).

R. Benoit is with the Sensors and Electron Devices Directorate, Army Research Lab, Adelphi, MD, USA (e-mail: Robert.r.benoit7.civ@mail.mil).

Y. Qiu is with the Liverpool John Moores University, Liverpool L3 3AF (e-mail: Y.Qiu@ljmu.ac.uk).

S. Cochran is with the University of Glasgow, Glasgow G12 8QQ, U.K. (e-mail: sandy.cochran@glasgow.ac.uk).

H. Lay is with FUJIFILM VisualSonics, Inc., Toronto, M4N 3N1, Canada (e-mail: holly.susan.lay@gmail.com).

S. Tiwari and R. Pratap are with the Department of Mechanical Engineering, Indian Institute of Science, Bangalore, India (e-mail: sudhanshut@iisc.ac.in; pratap@iisc.ac.in)

This article has been accepted for publication in a future issue of this journal, but has not been fully edited. Content may change prior to final publication. Citation information: DOI 10.1109/TUFFC.2019.2926211, IEEE Transactions on Ultrasonics, Ferroelectrics, and Frequency Control

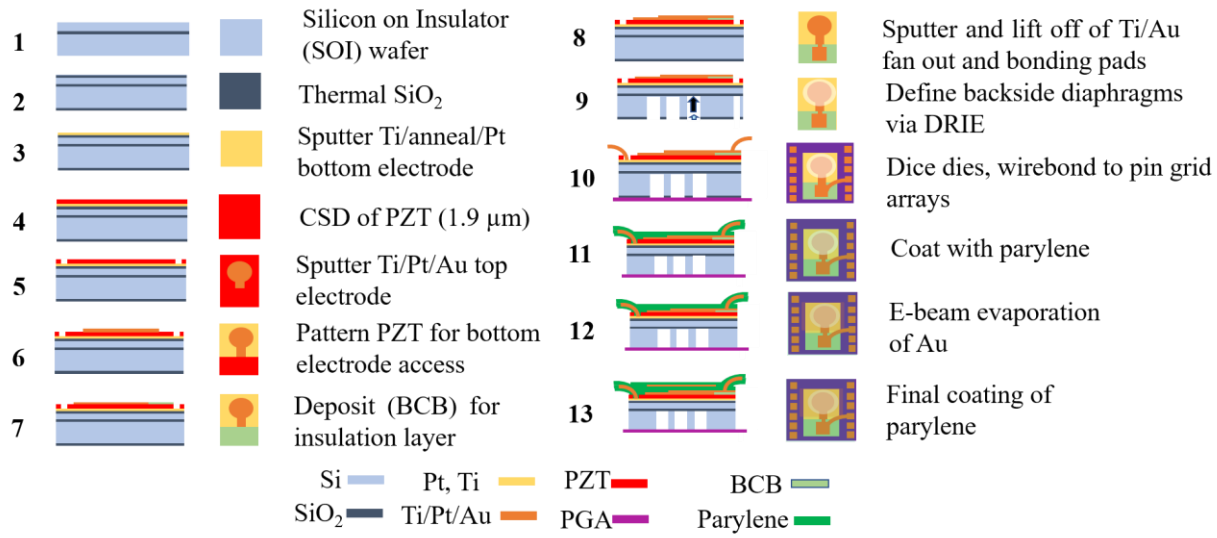

Fig. 2. PMUT fabrication process, with cross-sectional and top-view of the fabricated PMUT

CMUTs are based on flexural vibrations of a membrane caused by varying electrostatic attraction to a substrate. They can generate adequate acoustic pressures for medical imaging and particle trapping [9, 10]. They also integrate well with silicon electronics for voltage amplification and detection. However, they need high DC bias voltages (30 - 100 V) to operate, often near the collapse voltage, [11, 12] and this has led to interest in devices that do not require biasing. PMUTs, which accomplish membrane deflection through lateral strain induced by the piezoelectric effect, meet this need. Generally, they have higher capacitances than CMUTs and thus lower electrical impedance, facilitating impedance matching to electrical circuitry. In addition, unlike in bulk piezoelectric transducers, the resonant frequency of a PMUT is not dependent solely on the thickness of the piezoelectric layer but is defined by a range of parameters including density, flexural rigidity, diaphragm radius and shape of the membrane [8, 13, 14, 15]. Therefore, PMUTs offer significant freedom in their design.

Particle manipulation and trapping via acoustophoresis has been achieved in a variety of platforms, including transducers with interdigitated electrodes that use surface acoustic waves (SAW) to trap particles in the pressure wave antinodes [7, 16, 17], transducers that use standing bulk acoustic waves in a channel for droplet sorting [18], and single beam acoustic transducers (SBAT) for particle and cell manipulation [19, 20]. These techniques have demonstrated high efficiency in particle sorting and trapping. SAW-based devices and SBAT often require higher voltage input or a power amplifier during operation (> 10 V_{pp} operation) [20, 21], and the manipulation is often confined to a few wavelengths away from the substrate. Similarly, SBAT requires higher voltage operations and are difficult to fabricate in arrays, and thus may not have the manipulation precision and design freedom of PMUTs. While particle trapping has recently been shown to be possible with CMUTs [9, 10], to date, it has not been extensively demonstrated with PMUTs. In addition, demonstrations of the important task of bulk manipulation of particles from element to element in an array has been demonstrated with MUTs only with heavy reliance on microfluidic flow, although there have been such demonstrations in bulk and thick film transducers [22, 23, 24, 25, 26]. Further, particles have been reported to agglomerate towards the center of MUT diaphragms when the MUT is excited at the fundamental resonant frequency [9, 10]. While this fundamental mode thus enables particle trapping, use of higher frequencies has not been extensively explored. If adequate pressures can be generated at higher modes, particles may be systematically manipulated in correspondence with the vibration mode of the diaphragm, allowing dynamic patterning with a single element.

In this paper, one-dimensional (1D) PMUT arrays of multiple elements, each comprising many diaphragms connected electrically in parallel, are demonstrated through their manipulation of 4 µm SiO_2 particles via acoustophoresis without the assistance of microfluidic flow. It is also shown that bead patterns can be formed outside the operating bandwidth of the devices, with formation of bead patterns taking place over a wide frequency range.

II. Design, Fabrication, and Experimental Setup

A. Design

The resonant frequency (fundamental mode) of a PMUT, f, with a circular clamped diaphragm is given by: [13, 14, 15]

$$f = {\alpha^2}/{a^2}\sqrt{{D_e}/{\sum_i \rho_i h_i}} \quad (1)$$

where α, a, D_e, ρ_i, and h_i are the frequency parameter constant (equal to ~ 3.196 for a clamped circular diaphragm), the radius of the PMUT, flexural rigidity of the diaphragm, density of the i^{th} material in the stack forming the diaphragm, and thickness of the i^{th} material, respectively. Based on (1) and the material stack described in Section II.B, a diaphragm diameter of 60 µm was chosen to achieve a fundamental resonant frequency, f_{fr} = 10 MHz. 10 MHz was selected due to half the wavelength of the fundamental frequency in water, $\lambda_{fr}/2 \approx 75$ µm, is at least

on the order of or larger than the dimensions of most cells, bacteria, and enzymes [27, 28, 29]. This increases the possibility of successful acoustophoretic manipulation. The diaphragms were separated by a 15 µm gap with a pitch of 75 µm, corresponding to $\lambda_{fr}/2$. The top electrode diameter was set to 65% of the diaphragm diameter to increase deflection [30, 31, 32].

B. Fabrication

The full fabrication process for a PMUT is shown in Fig. 2. The base substrate was a silicon on insulator (SOI) wafer with a 2 µm Si thickness and a 2 µm buried thermal oxide layer (Ultrasil Corporation, Hayward, California, USA). An SiO_2 passive elastic layer ~0.16 µm thick was grown on both sides of the wafer by wet oxidation. Then 30 nm of Ti was sputtered on the device side, followed by rapid thermal annealing with 10 sccm of oxygen flow for 15 minutes at 700 °C to form TiO_2. This generates a well oriented 100 nm bottom electrode layer when Pt is sputtered at > 500 °C [33].

To achieve the highly oriented (001) PZT films needed for optimal functional performance in applications, a thin $Pb(Zr_{0.52}Ti_{0.48})O_3$ sol-gel solution with 2% Nb and 20 mol% excess Pb (Mitsubishi Materials Corporation, Hyogo, Japan) was first spun on the wafer at 6000 rpm for 30 s as the seed layer [34, 35] . The seed layer was then pyrolyzed at 200 °C for 150 s before crystallization via rapid thermal annealing in a Pb-rich environment at 700 °C for 1 min. For the functional thin film PZT layer, 14 mol% lead excess $Pb(Zr_{0.52}Ti_{0.48})O_3$ solution doped with 2% Nb (Mitsubishi Materials Corporation, Hyogo, Japan) was spun on at 2750 rpm for 45 sec. The film was then pyrolyzed at 100 °C for 1 min and 300 °C for 4 min, followed by crystallization in a lead-rich rapid thermal annealer for 1 min at 700 °C. This process was repeated until a total thickness of 1.9 µm was achieved. Typically, 20 repeats were needed. Afterwards, a thin PbO capping layer was deposited at 6000 rpm for 45 sec with the same pyrolysis and crystallization steps as the PZT layers to remove pyrochlore from the surface of the film.

The top electrode was formed by sputtering 2 nm Ti as an adhesion layer followed by 50 nm of Pt without breaking vacuum. The top electrode was annealed at 600 °C for 1 min before an additional 500 nm of Au was deposited and patterned to complete the top electrode. Access to the bottom electrode in areas not covered by the top electrode was gained by ion milling. An insulation layer was created by spinning and curing 0.9 µm thick bis(benzocyclobutene) to reduce parasitic capacitance over the areas defining the fan out and bonding pads. These were subsequently patterned via liftoff and ~30 nm Ti and 500 nm Au was sputtered without breaking vacuum. The devices were then released via silicon deep reactive ion etching (DRIE).

The wafer was diced into individual PMUT dies. These were mounted in the cavity of a pin grid array (PGA) (Spectrum Semiconductor Materials, San Jose, California, USA) with silver paste to prevent water leakage from the backside. Electrical connections were made with wire bonding and coated conformally with ~4 µm of parylene for waterproofing. An equipotential plane was formed to eliminate dielectrophoresis in the particle manipulation experiments by depositing a 100 nm thin film of Au with e-beam evaporation. A second protective layer of parylene (~ 2 µm) was then coated onto the device. Prior to characterization of the PMUT and the particle manipulation experiments, the array elements were poled at twice the coercive field of the PZT films for 15 min at room temperature.

C. Experimental Setup

For particle manipulation experiments, two linear types of PMUT arrays were tested: a 1D array in which each element comprised one single diaphragm (referred to here as E1) and a 1D array in which each element consisting of twenty diaphragms (referred to here as E20). In each case, the PGA cavity was filled with distilled water with varying concentrations of 4 µm SiO_2 beads (Sigma Aldrich, St. Louis, Missouri, USA). SiO_2 beads with 4 µm diameter were chosen as they were readily available. The water/air interface at the top of the cavity served as an acoustic reflector to generate standing waves. The PMUT elements were driven with continuous sinusoidal waves of amplitude 5 V_{pp} and a 2.5 V DC offset unless otherwise stated.

III. Simulations

It has been reported that acoustic tweezing with a single beam CMUT source is based on gradient forces arising from the fluctuation of the generated pressure field when the source is activated. The gradient forces move particles to local/global acoustic pressure maxima or minima, depending on the properties of the particle [9, 10]. When a PMUT diaphragm is excited at resonance, the first mode results in the highest diaphragm deflection and highest pressure in the acoustic medium at the center and the least deflection and pressure at the periphery of the diaphragm. Therefore, the maximum acoustic potential gradient arises between the center and edge of the diaphragm.

To describe how the particles should move in a pressure field, the acoustic potential can be related to the acoustic radiation force, F_{rad}, via Gor'kov's model

$$F_{rad} = -V*[\frac{f_1}{2}\beta_m \nabla\langle p_s^2\rangle - \frac{3f_2}{4}\rho_m \nabla\langle v_s^2\rangle], \quad (2)$$

where V is the volume of the particle and the terms in the brackets relate to the acoustic potential, β_m is the compressibility of the medium in which the particle is suspended, ρ_m is the density of the medium, v_s is the acoustic velocity, and p_s is the pressure on the particle [9, 10, 36, 37, 38]. The terms f_1 and f_2 are coefficients given by

$$f_1 = 1 - \frac{\beta_s}{\beta_m}, \quad (3)$$

$$f_2 = \frac{2(\rho_s - \rho_m)}{2\rho_s + \rho_m}, \quad (4)$$

This article has been accepted for publication in a future issue of this journal, but has not been fully edited. Content may change prior to final publication. Citation information: DOI 10.1109/TUFFC.2019.2926211, IEEE Transactions on Ultrasonics, Ferroelectrics, and Frequency Control

where β_s and ρ_s are the compressibility and density of the particle, respectively [9, 10, 37, 38]. Equations (2) – (4) were defined in COMSOL Multiphysics (COMSOL Inc., Burlington, MA, USA) for a single PMUT diaphragm, with 4 µm SiO_2 beads as the particles to be manipulated.

The results in Fig. 3 show that when a diaphragm is excited, particles agglomerate at the center and close to the surface of the diaphragm, in areas of high acoustic pressure. Similar behavior is reported in the literature but with CMUTs as the ultrasound source [9, 10]. Fig. 4 shows the pressure fields generated by a pair of diaphragms, simulated with COMSOL. It can be seen that the pressure fields generated by individual diaphragms overlap with adjacent diaphragms. Also, the particle movement caused by one diaphragm in Fig. 3 draws particles as far as 200 µm from a diaphragm center. It was calculated from COMSOL that close to the PMUT surface, the acoustic force was approximately ~10 pN and the effect of gravity force is two orders of magnitude lower (~ 0.4 pN). At approximately 50 µm away from the PMUT surface, the acoustic force is on the same order of magnitude as the gravity force. Thus, the particles were expected to move very close to the PMUT surface. In addition, if the pressure field is sufficiently large in extent and the distance between elements is sufficiently close, beads can potentially move from one element to another without assistance from microfluidic flow. This possibility was deliberately increased by designing the PMUT elements with a pitch of 75 µm, corresponding to $\lambda_{fr}/2$ at 10 MHz in water.

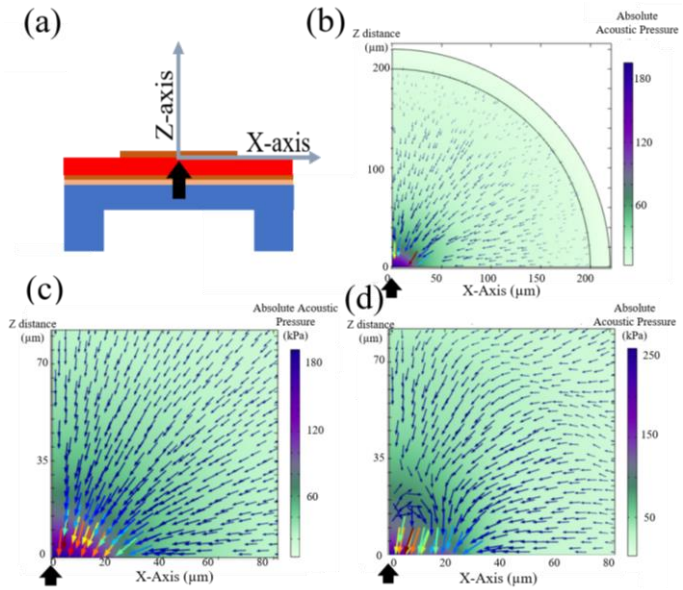

Fig. 3. Pressure fields generated by a single 60 µm diaphragm and particle movement for (b, c) fundamental mode and (d) second harmonic (0,2) mode. The arrows indicate the direction of SiO_2 beads particle movement. The colored arrows in (c, d) indicate the acoustophoretic force exerted on the particle. The length of the arrows corresponds to the relative force. The simulations were done for an axisymmetric model; only 1/2 of the diaphragm is shown, with the center at the origin as indicated by the black arrows. A point of reference is shown in (a). Note the model used was a planar simulation with symmetry along the out-of-plane axis. This X-Z view is also used for Fig. 4. A physically-matched layer was used at 200 µm distance from the membrane surface to prevent excitation of standing waves. An animation is presented in the Supplemental Materials.

In addition to those generated by the fundamental mode, patterns generated by different modes could potentially be useful. From the results shown in Fig. 3 and 4, different

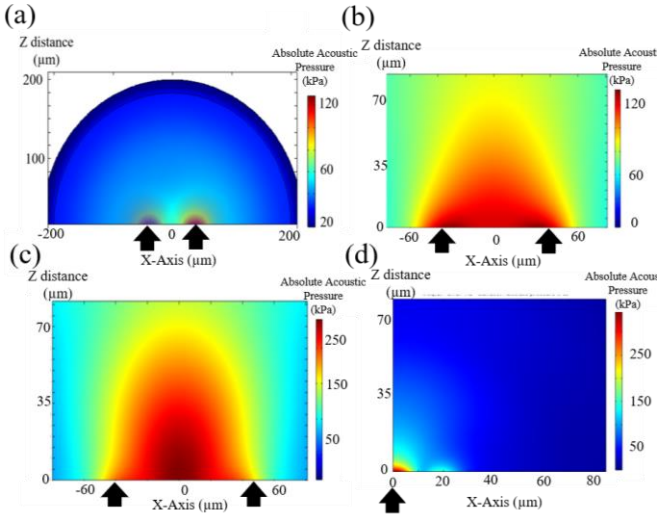

Fig. 4. (a) Individual pressure fields generated by two 60 µm diaphragms with 75 µm pitch, with each diaphragm excited individually and their individual pressure fields overlaid, (b) pressure field generated by two diaphragms excited in unison at resonance, (c) pressure field generated by two diaphragms excited in unison at 40% above the resonant frequency, and (d) pressure field generated by a single diaphragm excited at the second harmonic mode. The black arrows indicate the center of the diaphragms. The pressure fields overlapping in (a) and (b) indicate the potential for particles to move from one diaphragm to another. A physically-matched layer was used at 200 µm distance from the membrane surface to prevent excitation of standing waves

vibrational modes should generate different bead patterns based on the resultant pressure field. For example, the (0, 2) mode would occur at a frequency approximately 3.89 times the fundamental (0, 1) mode frequency of a clamped circular plate [39]. For the (0, 2) mode, the pressure field is shown in Fig. 3 (d) and 4 (d). This suggests there would be two areas where the beads could agglomerate: at the center of the diaphragm and in a circular node around the center of the diaphragm.

Figs. 3 and 4 were produced with a physically-matched layer positioned at 200 µm vertically from the membrane surface to prevent excitation of standing waves. If this is removed, allowing reflection, and the distance between the PMUT and the reflecting surface is multiple half-wavelengths, large pressure fields can be generated and correspondingly higher acoustic field amplitudes that can cause particles to move to levitation planes at the acoustical nodes [40]. The positions of the levitation planes (LPs) normal to the acoustic source direction can be expressed as

$$LP = n \cdot \lambda/4, \tag{5}$$

where n, and λ are a whole integer and the acoustic wavelength, respectively. The depth of the water in the PGA cavity was not controlled systematically in this study; however, levitation planes can be more readily formed if the cavity height is a multiple of the driving wavelength. Such planes increase in

This article has been accepted for publication in a future issue of this journal, but has not been fully edited. Content may change prior to final publication. Citation information: DOI 10.1109/TUFFC.2019.2926211, IEEE Transactions on Ultrasonics, Ferroelectrics, and Frequency Control

number if the driving frequency is high, as the number of nodal planes in a fixed distance increases with driving frequency.

IV. PMUT Characterization

For a high quality PMUT, the PZT quality needs to be high. X-ray diffraction (XRD) and field-emission scanning electron microscopy (FESEM) were used to confirm that the PZT films were phase-pure perovskites and highly (001) oriented as shown in Fig. 5. The relative permittivity, ε_r, and loss tangent, tan δ, were measured for twenty different elements in an array to test for the uniformity after the entire process was completed. Hysteresis loops were also measured to confirm the quality of the PZT. The electrical measurements are also presented in Fig. 5. At 95% confidence interval at 1 kHz, $\varepsilon_r = 1487 \pm 8$ and tan $\delta = 1.40 \pm 0.06$ %, respectively, indicating high uniformity between elements. The remanent polarization, P_r, was ≈ 24 μC/cm^2, and the coercive field, E_C, was ≈ 50 kV/cm.

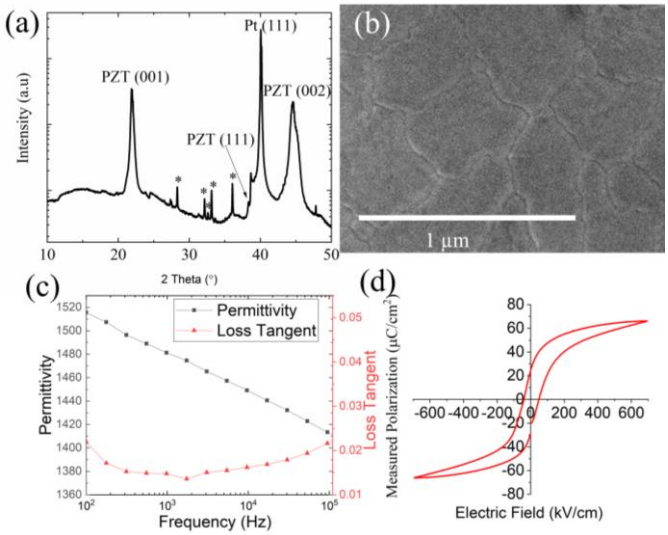

Fig. 5. Results of structural analysis of PZT via (a) X-Ray Diffraction and (b) Field Emission Scanning Electron Microscopy. Phase-pure perovskite was achieved with chemical solution deposition. No visible pyrochlore or secondary phases were found. The asterisks (*) denote substrate peaks. Measurements of (c) dielectric permittivity, loss tangent and (d) hysteresis loops indicate permittivity > 1400, loss tangent < 3%, remanent polarization ~24 μC/cm^2, and coercive field ~ 50 kV/cm.

Laser doppler vibrometry (LDV) was used to evaluate f_{fr} and the field-induced deflection of the fabricated device. The results are shown in Fig. 6. It was found that, for PMUTs on the same wafer, $6 < f_{fr} < 8$ MHz, due primarily to the footing effect in the DRIE process which changes the diaphragm diameter. Within a given die, the values of f_{fr} were well-matched, with larger variations observed across the 4" wafer. Higher modes can also be seen at 13.0 MHz and 19.8 MHz, which correspond to the (1, 1) and (0, 2) modes, respectively [39]. The LDV instrument (Polytec GmbH, Walbronn, Germany) could record a maximum deflection signal of only 79 nm, hence, for higher driving voltages, the center deflections seen in Fig. 6(b) were extrapolated from the deflections near the diaphragm periphery, where motion is more strongly clamped. Using this technique, the deflection profiles indicate that in air, high deflections (~ 40 nm/V) can be achieved for low driving voltages for both the E1 and E20 array.

The pressure output, *P*, and bandwidth, *BW*, were evaluated for the E20 array. The array was placed in an acrylic water-tank

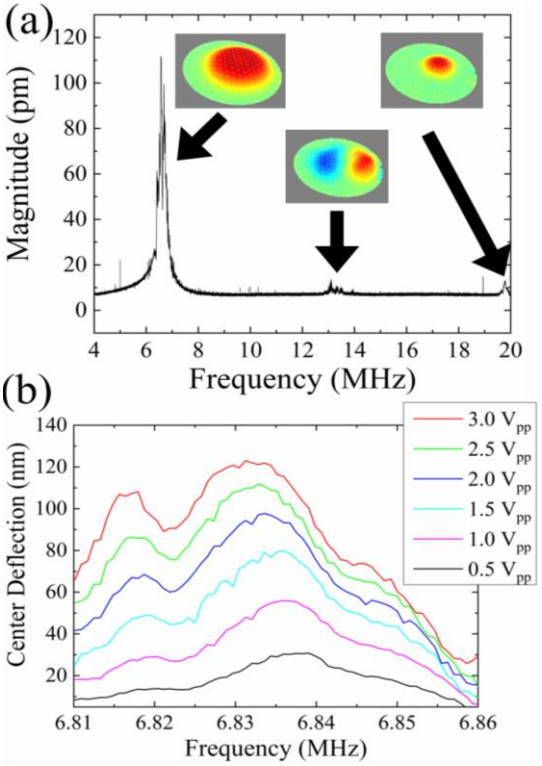

Fig. 6. LDV measurements in air showing center deflection spectra (a) over a wide frequency range at 0.5 – 3.0 V_{pp} driving voltage via laser chirp measurement and (b) close to resonance via peak hold measurement. Higher frequency modes are seen in (a) at 13 MHz and 19.5 MHz. The measurements here were from the same batch of devices used in later experiments.

and operated in transmit mode while a hydrophone (HGL-0085, Onda Inc., Sunnyvale, California, USA) acted as a receiver at 7.5 mm distance from the surface of the transducer. One element was excited with a 5 V_{pp} unipolar sinusoidal burst of 5 cycles to measure *P*. For *BW*, the same unipolar voltage excitation was used but with a single cycle sinusoid at the resonant frequency, and a total of 59 dB gain was used to amplify the signal. A Fourier transform was then used to calculate BW at -6 dB. The results are shown in Fig. 7. An element of 20 diaphragms (E20) yielded an output pressure of ~ 9.5 kPa at 7.5 mm and the bandwidth at -6 dB was approximately 62.5%. The underwater resonance frequency was found to be ~ 8 MHz.

This article has been accepted for publication in a future issue of this journal, but has not been fully edited. Content may change prior to final publication. Citation information: DOI 10.1109/TUFFC.2019.2926211, IEEE Transactions on Ultrasonics, Ferroelectrics, and Frequency Control

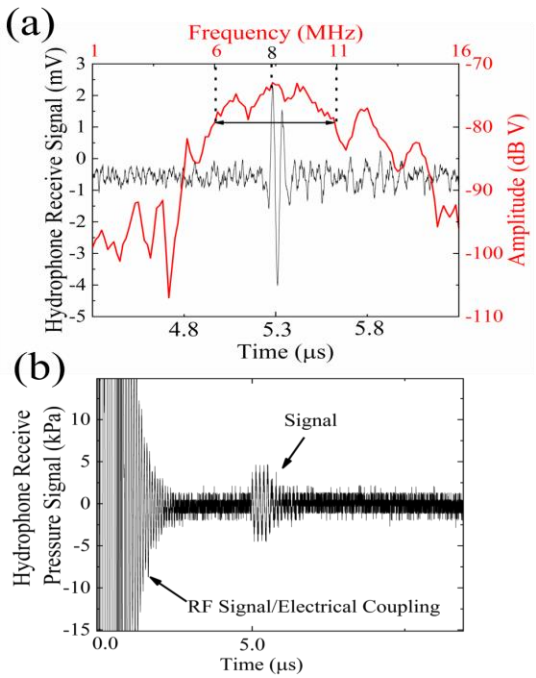

Fig. 7. Acoustic characterization of E20 array. (a) Time and frequency characteristics with single cycle sinusoidal excitation (with 59 dB total gain), and (b) hydrophone output at f_{fr} with 5 cycle sinusoidal excitation. The response was ~0.46 μV which corresponds to ~9.5 kPa at 5 V_{pp} unipolar excitation at 7.5 mm distance from the PMUT. The bandwidth at -6dB was ~ 62.5% from the Fourier transformation of the signal response, with a center frequency of 8 MHz.

V. Particle Manipulation

For particle manipulation experiments, the PMUT elements were excited below f_{fr} with a unipolar signal at 5 V_{pp} with a function generator, with a low concentration of 4 μm SiO_2 beads in the water medium. Results are shown in Fig. 8. The lower frequency was used because, when an element is excited very close to the resonant frequency, as presented in Fig. 8 (a) and (b), cross-coupling excited neighboring elements. At driving frequencies ~ 18% below f_{fr}, the cross-coupling was much less severe.

It was observed that the bead clusters became more tightly packed, as seen in Fig. 8 (c) and (d), as the applied unipolar voltage increased from 1 V_{pp} to 5 V_{pp} with $f \approx f_{fr}$. Furthermore, the velocity of the beads towards the axis of the diaphragm increased as the excitation voltage increased and when f_{fr} was approached. This is reasonable [9, 10] as higher deflections result in larger pressure outputs, generating larger pressure gradients and thus larger acoustic forces. The phenomenon of bead agglomeration towards the center of the diaphragm as the driving frequency approaches the resonant frequency corresponds with what has been reported for CMUTs [9, 10]. PMUTs which were not released by back side etching yielded no movement of the particles, showing that the particle manipulation arises from acoustophoresis.

In order to test control of particle motion in 1D, individual and adjacent elements of the E1 PMUT array were excited and non-excited to facilitate particles moving to the generated local acoustic potential minimum. A similar excitation pattern was used on the E20 PMUT array to investigate whether particle trapping is possible over multiple diaphragms simultaneously when one array element was excited. The results are presented in Fig. 9.

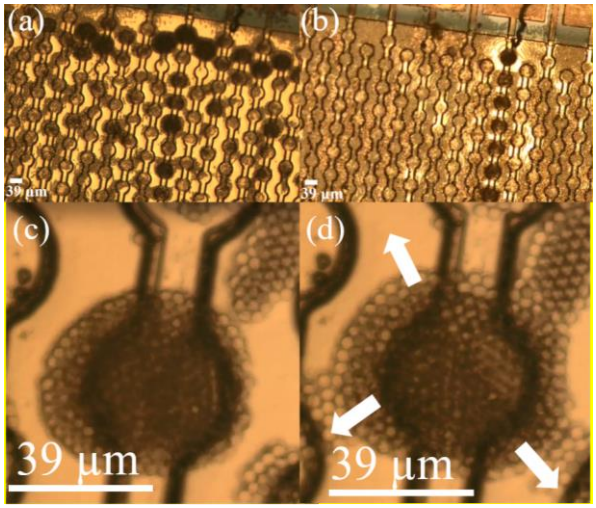

Fig. 8. SiO_2 bead patterns generated when the E20 array was excited at (a) ~6 MHz, (b) ~ 4.9 MHz. Cross-coupling is less severe below resonance, indicated by the much heavier clustering of particles at the excited element. Generally, the beads agglomerated most effectively with f in the range 5 – 6 MHz. Higher density particle clustering was observed for (c) 5 V_{pp} excitation than for (d) 1 V_{pp} excitation; higher voltages caused tighter conglomeration of the beads than lower voltages. The white arrows indicate the direction that as voltage is decreased, the bead cluster relaxed and the diameter of the cluster decreased from (c) to (d) from ~ 60 μm to ~54 μm, respectively.

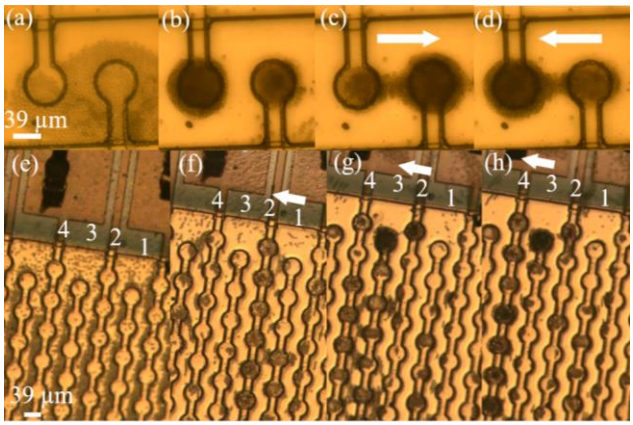

Fig. 9. Manipulation of 4 μm silica beads using two elements from the E1 (a) – (d) and E20 (e) – (h) PMUT designs. The images show the SiO_2 beads when (a) elements are off, (b) both elements are turned on, (c) when the left element is switched off and the right element remains on, and (d) when the right element is switched off and the left element is switched on. Beads move from the element that is turned off to the element that is turned on. This technique was used when manipulating the beads with the E20 design, where beads were trapped and moved from element 1 to element 4. The white arrows indicate the direction of particle movement. Note the scalebars are consistent between (a) – (d) and (e) – (h).

When an element is turned on, nearby beads cluster over the center of the diaphragm and, when the element is turned off, the bead cluster disperses and moves toward neighboring elements that remain activated, due to the gradient in acoustic pressure, in agreement with the simulations presented in Figs. 3 and 4.

This article has been accepted for publication in a future issue of this journal, but has not been fully edited. Content may change prior to final publication. Citation information: DOI 10.1109/TUFFC.2019.2926211, IEEE Transactions on Ultrasonics, Ferroelectrics, and Frequency Control

This behavior was observed for both the E1 and E20 arrays. Because the pressure gradient increases between the center of a diaphragm and its periphery as f approaches f_{fr} [9, 10], the beads can be moved from one element to another by tuning the driving frequency. The relationship between frequency and wavelength and particle movement is complex; changing frequency results in changing deflection, which changes output pressure as well as potential crosstalk, further complicating the acoustic potential gradient. In addition, changing frequency also changes wavelength, and thus also changes the acoustic potential gradient. However, based on Fig. 4 (c), when two diaphragms are excited above the resonant frequency, the area of highest pressure is between two diaphragms rather than directly over the diaphragms. By exciting the transducers at a frequency above resonance, the beads move to the highest areas of pressure, and thus move to the areas between the two diaphragms. Then, the driving frequency can be changed to the resonant frequency, and thus the beads move to areas over the diaphragm easier due to closer proximity to the generated highest-pressure zone, as was observed in the experiments.

The effects of different excitation frequencies on bead patterns and behavior over diaphragms in the E1 and E20 arrays are illustrated in Figs. 10 and 11, respectively. For the E1 array, again the beads agglomerate at the center of the diaphragm at f_{fr}. The beads remain at the center of the diaphragm until $f \approx 17$ MHz, where they begin to form an annulus. As f approaches 23 MHz, two beads move towards the center of the diaphragm, while most stay in the nodal torus formed previously. The pattern in which the torus appears matches the simulated pressure field generated by the (0,2) mode shown in Fig. 4 (d). If the resonant frequency is taken to be ~ 6 MHz (at which frequency the beads tended to agglomerate most effectively), 23 MHz is approximately 3.9 times f_{fr}, again matching theory [39]. The (1,1) mode was not seen via bead excitation. The in-plane stress in the piezoelectric layer induced by the electric field produces a uniform bending moment along the periphery of the top electrode. This favors radial modes instead of non-radial modes; hence, the amplitude of the (1,1) mode may be too low to cause acoustophoretic motion of beads [15, 39].

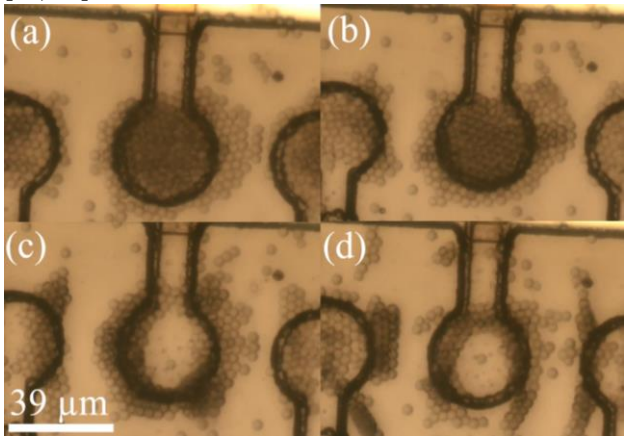

Fig. 10. Particle behavior stimulated by driving one element at frequencies (a) 5 MHz, (b) 13 MHz, (c) 17 MHz, and (d) 23 MHz. The scalebar applies to all of (a) – (d).

For the E20 device, similar patterns emerged; beads agglomerated at the center of each diaphragm when resonance was approached, and torus shapes were seen at approximately $f \approx 3.9 f_{fr}$. However, several unique behaviors were seen in elements with 20 diaphragms compared to elements with only 1 diaphragm, as shown in Fig. 11. Beads moved away from the excited diaphragm at 7 MHz, and returned at 8 MHz. This behavior was also seen when transitioning from 9 MHz to 13 MHz. One possible explanation can be drawn from the simulation illustrated in Fig. 4 (c), where above f_{fr}, an acoustic potential well can encourage beads to move away from the diaphragm. When the elements are excited together, depending on the separation distance between elements and the excitation frequency, larger acoustic pressures may be generated between diaphragms, with the resulting gradient pushing the beads towards the higher-pressure regions. Crosstalk from neighboring, non-electrically excited elements may thus be the cause of behaviors seen in Fig. 11 (c)-(d), (e)-(f), and (g)-(h).

At higher driving frequencies, even without precise control over the height of the chamber, levitation planes were also observed, as shown in Fig. 12, with the heights of the levitation planes indicated in Table I.

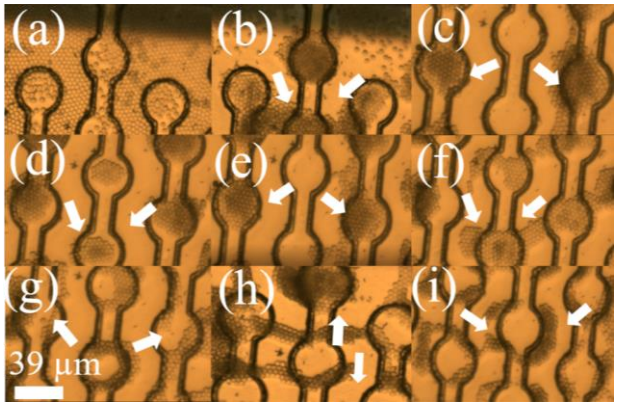

Fig. 11. Silica bead patterns generated using E20 with driving frequencies at (a) 1 MHz, (b) 3 – 6 MHz, (c) 7 MHz, (d) 8 MHz, (e) 9 MHz, (f) 13 MHz, (g) 17 MHz, (h) 18 MHz, (i) 22 MHz. Arrows indicate directions of particle motion before the particles settle into their observed position. The scalebar applies to (a) – (i).

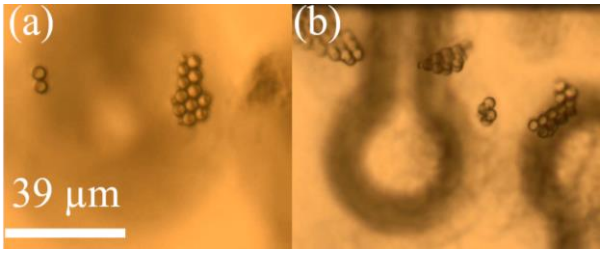

Fig. 12. Levitation plane of 4 µm SiO_2 beads when PMUTs E1 were excited at (a) 30 MHz and (b) 50 MHz. The levitation planes are identified in Table I. The levitation planes are evident due to the need to defocus the microscope from the PMUT surface and focus on areas above it. The scalebar applies to (a) and (b).

In some cases, multiple levitation planes were observed. The levitation planes form at heights that correspond approximately with $n\lambda/4$ as predicted by Equation (5). While the beads are trapped in the levitation plane, they have little motion in the X and Y directions. It is noteworthy that these effects were observed far beyond the limits of the measured BW of 62.5%.

This article has been accepted for publication in a future issue of this journal, but has not been fully edited. Content may change prior to final publication. Citation information: DOI 10.1109/TUFFC.2019.2926211, IEEE Transactions on Ultrasonics, Ferroelectrics, and Frequency Control

TABLE I
LEVITATION PLANE HEIGHTS AT DIFFERENT EXCITATION FREQUENCIES

Driving Frequency (MHz)	Half wavelength value (μm)	Observed Levitation Plane Heights (from PMUT surface, μm)
30	25	56, 74
50	15	19, 38, 51
60	12.5	10, 20

VI. CONCLUSIONS

PMUT arrays were successfully fabricated with high quality (001) oriented PZT that produced ~ 9.5 kPa at 7.5 mm distance and 40 nm/V deflection in air at 6 – 8 MHz resonant frequency. The arrays were shown to have the ability to control the location of SiO_2 beads and bead agglomerations in 1D (laterally) by selecting which PMUTs were excited. At higher excitation frequencies, different bead patterns were observed, with the potential for use for patterning cells and particles in ways other than the agglomeration at the diaphragm center demonstrated previously with CMUTs [9, 10]. Even well above the -6 dB bandwidth of the fundamental resonant mode, levitation planes and bead patterning were observed, demonstrating generation of sufficient pressure to realize these effects at frequencies as high as 60 MHz.

This work opens a pathway towards 2D manipulation of particles via PMUT arrays. Of particular interest would be to assess whether asymmetric nanorods, cells, and proteins / enzymes can be manipulated with PMUTs. While preliminary data shows that biological cells move upon activation of the PMUT, it was difficult to deterministically manipulate the cells from element to element. This was attributed to the acoustic impedance mismatch between the medium (distilled water) and cells being much lower compared to distilled water and silica beads, and is thus difficult to manipulate with the current pressure outputs. In the future, this can be circumvented by either increasing the drive voltages, improving PMUT pressure output, or by manipulating bubbles in conjunction with the cells, which has been demonstrated in literature [41]. In addition, PMUTs integrated into device apparatuses for imaging will also be explored in the future.

APPENDIX

Videos of particle manipulation are available online.

ACKNOWLEDGEMENTS

The authors thank Dr. Christine Démoré at Sunnybrook Research Institute, Toronto, Ontario, Canada, for technical discussions.

REFERENCES

[1] J. Hultström, O. Manneberg, K. Dopf, H. M. Hertz, H. Brismar, M. Wilund. "Proliferation and viability of adherent cells manipulated by standing-wave ultrasound in a microfluidic chip," *Ultrasound in Med. & Biol.*, vol. 33, no. 1, pp. 145-151, Dec. 2007.

[2] D. Carugo, D. Ankrett, P. Glynne-Jones, L. Capretto, R. J. Boltryk, X. Zhang, P. Townsend, and M. Hill. "Contrast agent-free sonoporation: The use of an ultrasonic standing wave microfluidic system for the delivery of pharmaceutical agents," *Biomicrofluidics*, vol. 5, no. 4, Art. No. 004108.

[3] M. Ziskin and D. Petitti. "Epidemiology of human exposure to ultrasound: A critical review," *Ultrasound in Med. & Biol.*, vol. 14, no. 2, pp. 91-96, 1988.

[4] M. Wiklund, T. Laurell and A. Lenshof. "Biocompatibility and cell viability in acoustofluidic resonators," in *Microscale Acoustofluidics*, Cambridge, UK: The Royal Society of Chemistry, 2015, ch. 21, sec. 4. pp. 545 – 562. [Online]. Available: https://pubs.rsc.org.

[5] M. Evander, L. Johansson, T. Lilliehorn, J. Piskur, M. Lindvall, S. Johansson, M. Almqvist, T. Laurell, and J. Nilsson. "Noninvasive acoustic cell trapping in a microfluidic perfusion system for online bioassays.," *Anal. Chem.*, vol. 79, no. 7, pp. 2984-2991, Feb. 2007.

[6] M. Wiklund, "Acoustofluidics 12: Biocompatibility and cell viability in microfluidic acoustic resonators," *Lab Chip*, vol. 12, no. 11, pp. 2018-2028. May 2012.

[7] F. Guo, Z. Mao, Y. Chen, Z. Xie, J. Lata, P. Li, L. Ren, J. Liu, J. Yang, M. Dao, S. Suresh, and T. Huang. "Three-dimensional manipulation of single cells using surface acoustic waves," *Proc. Natl. Acad. Sci. U.S.A.*, vol. 113, no. 6, pp. 1522-1527. Jan. 2016.

[8] Y. Qiu, J. V. Gigliotti, M. Wallace, F. Griggio, C. Demore, S. Cochran, and S. Trolier-McKinstry. "Piezoelectric micromachined ultrasound transducer (PMUT) arrays for integrated sensing, actuation, and imaging," *Sensors*, vol. 15, no. 4, pp. 8020-8041. Apr. 2015.

[9] C. Samarasekera, J. G. W. Sun, Z. Zheng, and J. T. W. Yeow. "Trapping, separating, and palpating microbead clusters in droplets and flows using capacitive micromachined ultrasonic transducers (CMUTs)," *Sensors & Actuators: B. Chemical*, vol. 276, pp. 481-488 Aug. 2018.

[10] S. P. Mao, K. Zhong, V. Rochus, S. Severi, B. Nauwelaers, H. A. C. Tilmans, and X. Rottenberg. "Capacitive micromachined ultrasonic transducers for acoustic manipulation," in *18th International Conference on Solid-State Sensors, Actuators and Microsystems (Transducers)*, Anchorage, AK, USA, 2015, pp. 662-665.

[11] A.S. Ergun, G. G. Yaralioglu, and B. T. Khuri-Yakub, "Capacitive Micromachined Ultrasonic Transducers: Theory and Technology," *Journal of Aerospace Engineering*, vol. 16, no. 2, 76-84. Nov. 2002.

[12] A. Nikoozadeh, B. Bayram, G. G. Yaralioglu, B. T. Khuri-Yakub, "Analytical calculation of collapse voltage of CMUT membrane [capacitive micromachined ultrasonic transducers]," in *IEEE Ultrasonics Symposium*, Montreal, Quebec, Canada, 2004, pp. 256-259.

[13] F. Sammoura, K. Smyth, S. Bathurst, and S. Kim. "An analytical analysis of the sensitivity of circular piezoelectric micromachined ultrasonic transducers to residual stress," in *Proc. IEEE International Ultrasonics Symposium*, Dresden, Germany, 2012, pp. 580-583.

[14] A. Dangi and R. Pratap. "System level modeling and design maps of PMUTs with residual stresses," *Sensors and Actuators A: Physical*, vol. 262, pp. 18-28, May 2017.

[15] S. Timoshenko and S. Woinowsky-Krieger, *Theory of plates and shells*. Singapore: McGraw-Hill, 1959, pp. 1-568.

[16] L. Ren, S. Yang, P. Zhang, Z. Qu, Z. Mao, P. Huang, Y. Chen, M. Wu, L. Wang, P. Li, and T. Huang, "Standing Surface Acoustic Wave (SSAW)-Based Fluorescence-Activated Cell Sorter," *Small*, vol. 14, no. 40, pp. 1801996, Oct. 2018.

[17] M. Wu, K. Chen, S. Yang, Z. Wang, P. Huang, J. Mai, Z. Li, and T. Huang, "High-throughput cell focusing and separation *via* acoustofluidic tweezers," *Lab on a Chip*, vol. 18, pp. 3003-3010, Aug. 2018.

[18] I. Leibacher, P. Reichert, and J. Dual, "Microfluidic droplt handling by bulk acoustic wave (BAW) acoustophoresis," *Lab on a Chip*, vol. 15, pp. 2896-2905, Jun. 2015.

[19] K. Lam, Y. Li, Y. Li, H. Lim, Q. Zhou, and K. Shung, "Multifunctional single beam acoustic tweezer for non-invasive cell/organism manipulation and tissue imaging," *Scientific Reports*, vol. 6., no. 37554, Nov. 2016.

[20] B. Zhu, J. Xu, Y. Li, T. Wang, K. Xiong, C. Lee, X. Yang, M. Shiiba, S. Takeuchi, Q. Zhou, and K. Shung, "Micro-particle manipulation by single beam acoustic tweezers based on hydrothermal PZT thick film," *AIP Advances*, vol. 6, no. 35102, Mar. 2016.

[21] S. Li, X. Ding, Z. Mao, Y. Chen, N. Nama, F. Guo, P. Li, L. Wang, C. Cameron, and T. Huang, "Standing surface acoustic wave (SSAW)-based cell washing," *Lab Chip*, vol. 15, no. 1, pp. 331-338, Jan 2015.

[22] A. Marzo and B. W. Drinkwater, "Holographic acoustic tweezers," *Proceedings of the National Academy of Sciences of the United States of America*, vol. 116, no. 1, pp. 84-89. Dec. 2018.

[23] S. Deng, K. Jia, E. Wu, X. Hu, Z. Fan, and K. Yang, "Controllable Micro-Particle Rotation and Transportation Using Sound Field Synthesis Technique," *Applied Sciences*, vol. 8, no. 1, pp. 73, Jan. 2018.

[24] Y. Qiu, H. Wang, S. Gebhardt, A. Bolhovitins, C. Démoré, A. Schönecker, S. Cochran, "Screen-printed ultrasonic 2-D matrix array transducers for microparticle manipulation," *Ultrasonics*, vol. 62, pp. 136-146, Sept. 2015.

[25] C. Yoon, B. J. Kang, C. Lee, H. H. Kim, and K. K. Shung, "Multi-particle trapping and manipulation by a high-frequency array transducer," *Applied Physics Letters*, vol. 105, no. 21, pp. 21403, Nov. 2014.

[26] H. Wang, Y. Qiu, C. Démoré, S. Gebhardt, and S. Cochran, "2-D crossed-electrode transducer arrays for ultrasonic particle manipulation," in *IEEE International Ultrasonics Symposium*, Tours, France, Sept. 2016.

[27] N. Nama, R. Barnkob, Z. Mao, C. Kähler, F. Costanzo, and T. Huang, "Numerical study of acoustophoretic motion of particles in a PDMS microchannel driven by surface acoustic waves," *Lab Chip*, vol. 15, no. 12, pp. 2700-2709, May 2015.

[28] M. Antfolk, P. B. Muller, P. Augustsson, H. Bruus, and T. Laurell, "Focusing of sub-micrometer particles and bacteria enabled by two-dimensional acoustophoresis," *Lab Chip*, vol. 12, no. 15, pp. 1210-1223, May 2014.

[29] Y. Liu and K. Lim, "Particle separation in microfluidics using a switching ultrasound field," *Lab on a Chip*, vol. 11, no. 18, pp. 3167-3173, Aug 2011.

[30] P. Muralt and J. Baborowski, "Micromachined ultrasonic transducers and acoustic sensors based on piezoelectric thin films," *Journal of Electroceramics*, vol. 12, no. 1-2, pp. 101-108, Jan. 2004.

[31] R. J. Przybyla, "Ultrasonic 3D Rangefinder on a chip," Ph.D. dissertation, Dept. Elect. Eng., University of California, Berkeley, Berkeley, CA, USA, 2013.

[32] Y. Lu and D. A. Horsley, "Modeling, fabrication, and characterization of piezoelectric micromachined ultrasonic transducer arrays based on cavity SOI wafers," *Journal of Microelectromechanical Systems*, vol. 24, no. 4, pp. 1142-1149, Jan. 2015.

[33] A. J. Fox, B. Drawl, G. R. Fox, B. J. Gibbons, S. Trolier-McKinstry, "Control of crystallographic texture and surface morphology of Pt/TiO_2 templates for enhanced PZT thin film texture," *IEEE Transactions on Ultrasonics, Ferroelectrics, and Frequency Control*, vol 62, no. 1, pp. 56-61, Jan. 2015.

[34] T. M. Borman, S. W. Ko, P. Mardilovich, S. Trolier-McKinstry, "Development of crystallographic texture in chemical solution deposited lead zirconate titanate seed layers," *Journal of the American Ceramic Society*, vol. 100, no. 10, pp. 4476-4482, Oct. 2017.

[35] T. M. Borman, W. Zhu, K. Wang, S. W. Ko, P. Mardilovich, S. Trolier-McKinstry, "Effect of lead content on the performance of niobium-doped {100} textured lead zirconate titanate films," *Journal of the American Ceramic Society*, vol. 100, no. 8, pp. 3558-3567, Aug. 2017.

[36] L. Gorkov, "On the forces acting on a small particle in an acoustical field in an ideal fluid," *Sov. Phys. Dokl. (Engl. Transl.)*, vol. 6. Pp 773. Mar. 1962.

[37] S. V. V. N. Kothapalli, M. Wiklund, B. Janerot-Sjoberg, G. Paradossi, and D. Grishenkov. "Investigation of polymer-shelled microbubble motions in acoustophoresis," *Ultrasonics*, vol. 70, pp. 275-283. June 2016.

[38] H. Bruus, "Acoustofluidics 7: The acoustic radiation force on small particles," *Lab Chip*, vol. 12, no. 6. pp. 1014-1021

[39] A. W. Leissa, *Vibration of plates.* Washington D.C.: U.S. Government Printing Office, 1969, pp. 1-345.

[40] S. Zhao and J. Wallaschek, "A standing wave acoustic levitation system for large planar objects," *Arch Appl Mech*, vol. 81, no. 2, pp. 123-139, Dec. 2009.

[41] A. van Wamel, A. Bouakaz, M. Versluis, and N. de Jong, "Micromanipulation of endothelial cells: Ultrasound-microbubble-cell interaction," *Ultrasound in Medicine & Biology*, vol. 30, no. 9, pp. 1255-1258. Sept. 2004.